Atmospheric
Chemistry
and Physics

Supplement of

New particle formation in the tropical free troposphere during CAMP²Ex: statistics and impact of emission sources, convective activity, and synoptic conditions

Qian Xiao et al.

Correspondence to: Jian Wang (jian@wustl.edu)

Supplementary Information

1 Estimation of UV actinic flux from irradiance

To evaluate the actinic flux during NPF events observed in the early morning (see Sect. 4.1), we estimated UV actinic flux from irradiance measurements, solar zenith angle (SZA), and sky condition (Kylling et al., 2003; Webb et al., 2002). When SZA is higher than 60º or under clear sky conditions, the downwelling irradiance is assumed as direct only (Kylling et al., 2003), and total actinic flux is given by:

$$E_{UV} = \frac{F_{dn}}{\cos(SZA)} + 2 \cdot F_{up} \qquad (S1)$$

Where E_{UV} represents actinic flux over the UV wavelength range, F_{dn} and F_{up} are the downwelling and upwelling components of UV irradiance. Under cloudy and overcast conditions, actinic flux is simply twice the sum of both components (Kylling et al., 2003). We utilized the zenith cloud mask data to help identify the cloud conditions, which is developed using the Cloud Detection Neural Network (CDNN; Nied et al., 2023) based on the forward camera onboard the aircraft. The UV irradiance and estimated actinic flux during the early morning NPF events (7:00-10:00, local time) are compared with those during NPF events observed around noon time (10:00-14:00, Fig. S4). The median UV irradiance during morning background NPF events is about 28% lower than that of the NPF events around noon, while the median UV actinic flux is about 11% lower.

2 NPF under very low CS conditions in the morning

One possible explanation for the background NPF in the early morning is that the new particles were formed the day before under high UV irradiance/actinic flux, survived scavenging overnight, and were detected in the morning. If that was the case, we expect that the CS at the time of NPF should be similar or even lower than the CS when the new particles were observed the next morning. This is because if the CS was reduced by wet scavenging after NPF, the newly formed particles would have been efficiently removed by coagulation with cloud droplets, and no NPF events would be identified the next morning. Because there are no continuous measurements from late afternoon to the next morning, we statistically compare the fraction of measurements with

very low CS (i.e., below 0.001 s^{-1}) and the NPF frequency between early morning (7:00-10:00 local time) and late afternoon (15:00-18:00 local time) above 5 km during the entire campaign (Fig. S5). The percentage of the data with CS below 0.001 s^{-1} in the early morning (i.e., 7:00-10:00) is about 22%, significantly higher than that in the late afternoon (4%, 15:00-18:00), indicating the condition of very low CS is much more prevalent during the early morning. In addition, the frequency of NPF in the early morning is about 20 times higher than that in the afternoon, suggesting that new particles observed were most likely formed in the morning, instead of the day before. Otherwise, the frequency of NPF in the afternoon would have exceeded or at least been comparable to that in the early morning.

3 NPF over coastal regions and land at altitudes of 5.5-6.5 km

Given the dependence of NPF on multiple parameters (e.g., CS, UV irradiance, and precursor concentrations), the potential impact of urban emissions on NPF is examined statistically. One approach is to statistically compare $N_{>3\ nm}/N_{>10\ nm}$ and $N_{3\text{-}10\ nm}$ between urban-influenced NPF (i.e., classified in cluster #1) and background NPF events under the same conditions (i.e., temperature, CS, RH, and UV irradiance). However, such comparison is not possible as most background NPF events observed at similar altitudes have substantially lower UV irradiance (below 100 W m^{-2}, cluster #2). As a result, the impact of urban emission on NPF was examined by statistically comparing urban influenced NPF and non-NPF events at the similar altitude range and time of the day (such that temperature and UV irradiance are at similar levels) as a function of CS. Figure S8 shows that urban influenced NPF occurred mostly with CS below 0.002 s^{-1}, substantially lower than during most of the non-NPF periods. For CS below 0.002 s^{-1}, the UV irradiances are statistically similar between urban influenced NPF events and non-NPF periods, whereas urban-influenced NPF events show elevated CH$_4$ concentration. This suggests that precursors emitted from urban areas likely contribute to the formation of nucleating species and NPF.
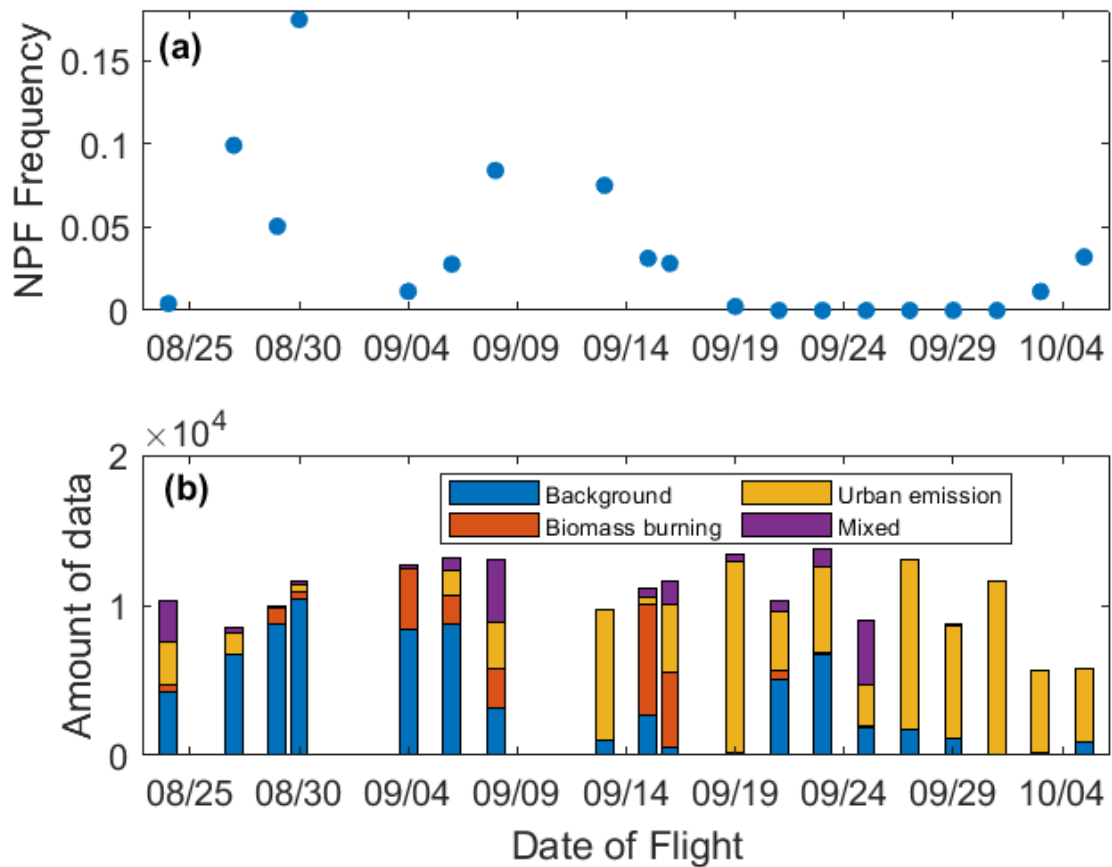
2

Figure S1. (a) NPF frequency (defined as the ratio of sampling time identified as NPF events to the total sampling time) for each flight and (b) the amount of data classified as different air mass types for each flight.
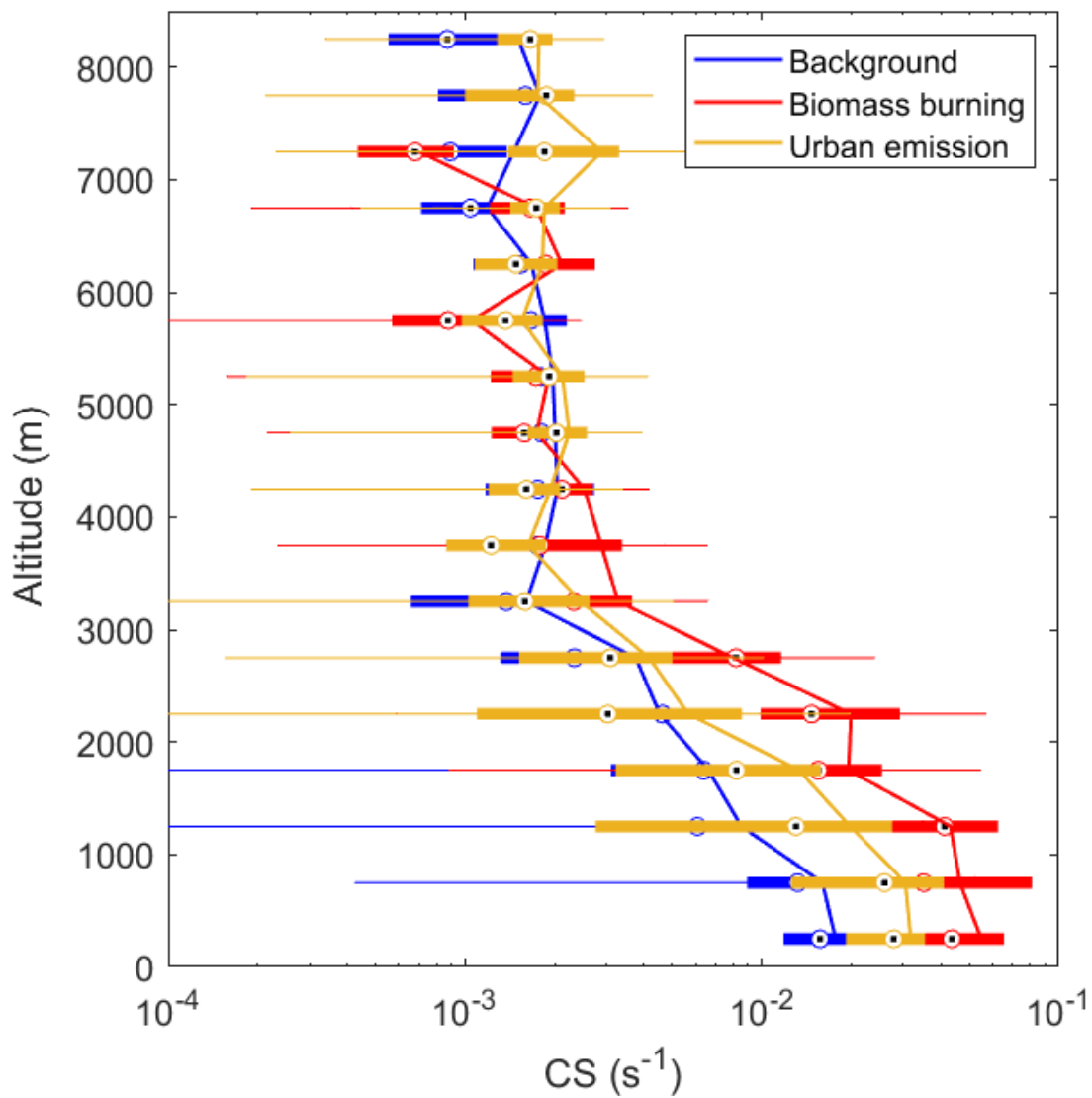
Figure S2. Vertical profiles of CS for three major air mass types during CAMP^{2}Ex. The lines represent the mean CS of the altitude bins. In-cloud data are excluded from the statistics.
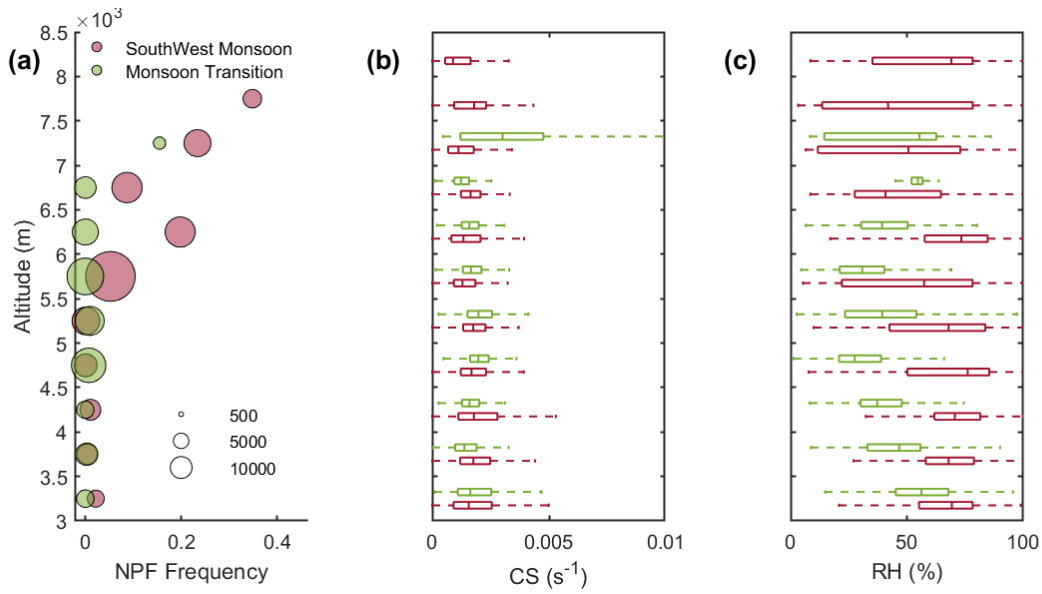
Figure S3. Comparison of vertical profiles between flights during southwest monsoon (RF1-RF11, 24 August to 20 September) and during monsoon transition (RF12-RF19, 20 September to 5 October) in terms of (a) NPF frequency, (b) CS, and (c) RH. The size of the circles refers to the amount of data sampled within the altitude bin.
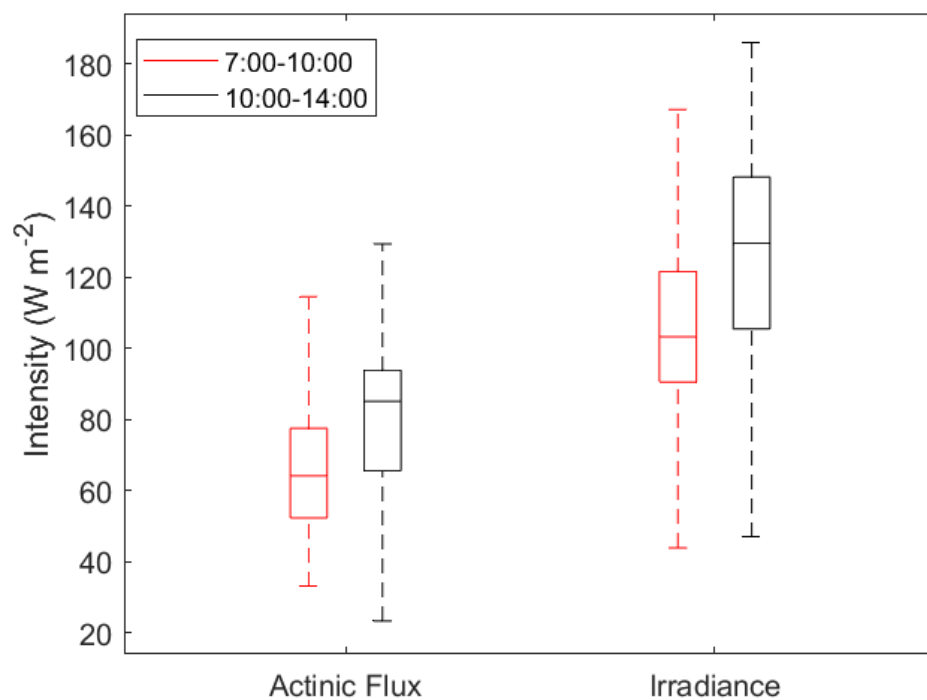
Figure S4. Statistical comparison of UV irradiance and estimated actinic flux during the early morning background NPF events (7:00-10:00, red) and those during NPF events observed around noon time (10:00-14:00, black) in the same altitude range (i.e., 6.5-7.2 km).
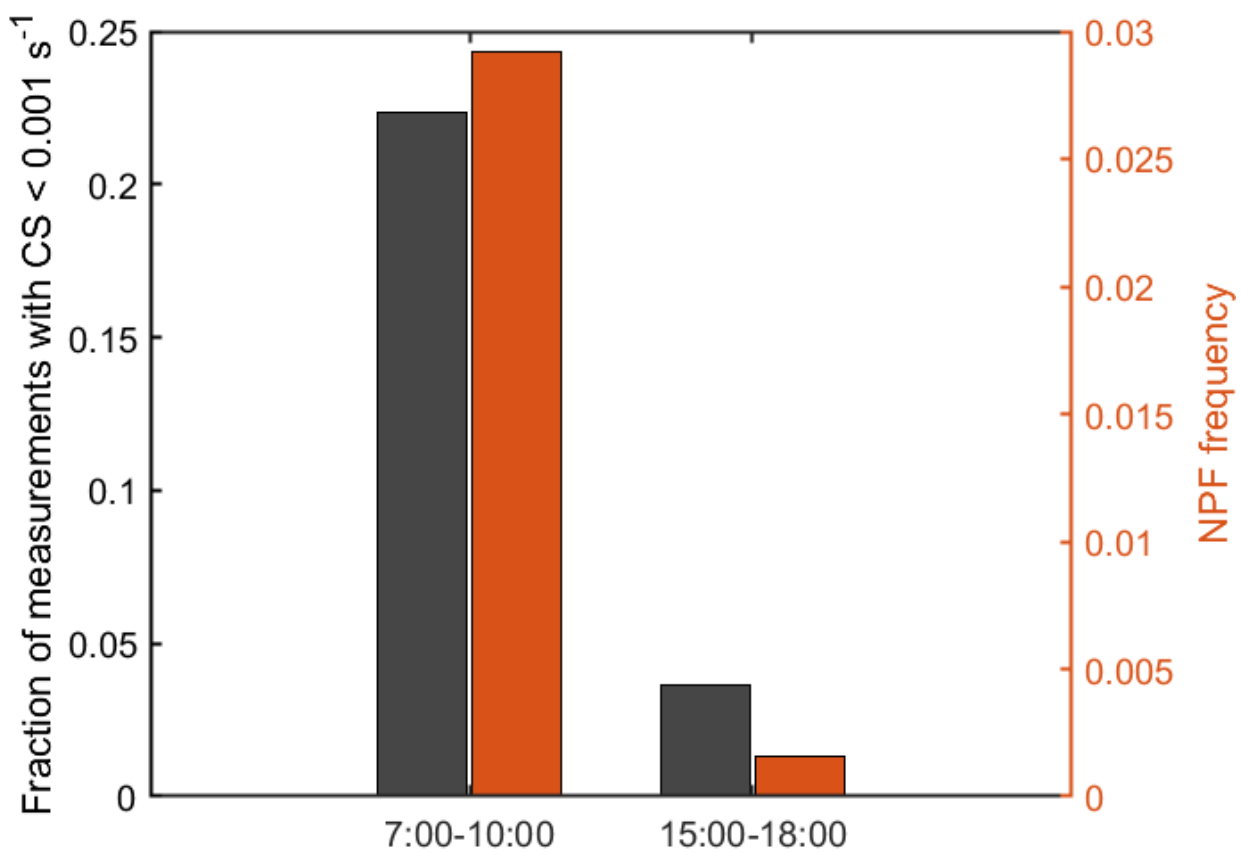
Figure S5. The fraction of measurements under very low CS condition (i.e., below 0.001 s^{-1}, black bars) and NPF frequency (red bars) in the early morning (7:00-10:00) and late afternoon (15:00-18:00). Measurements used in the calculation are out of clouds and above 5 km, where most NPF events were observed during the CAMP^{2}Ex campaign.
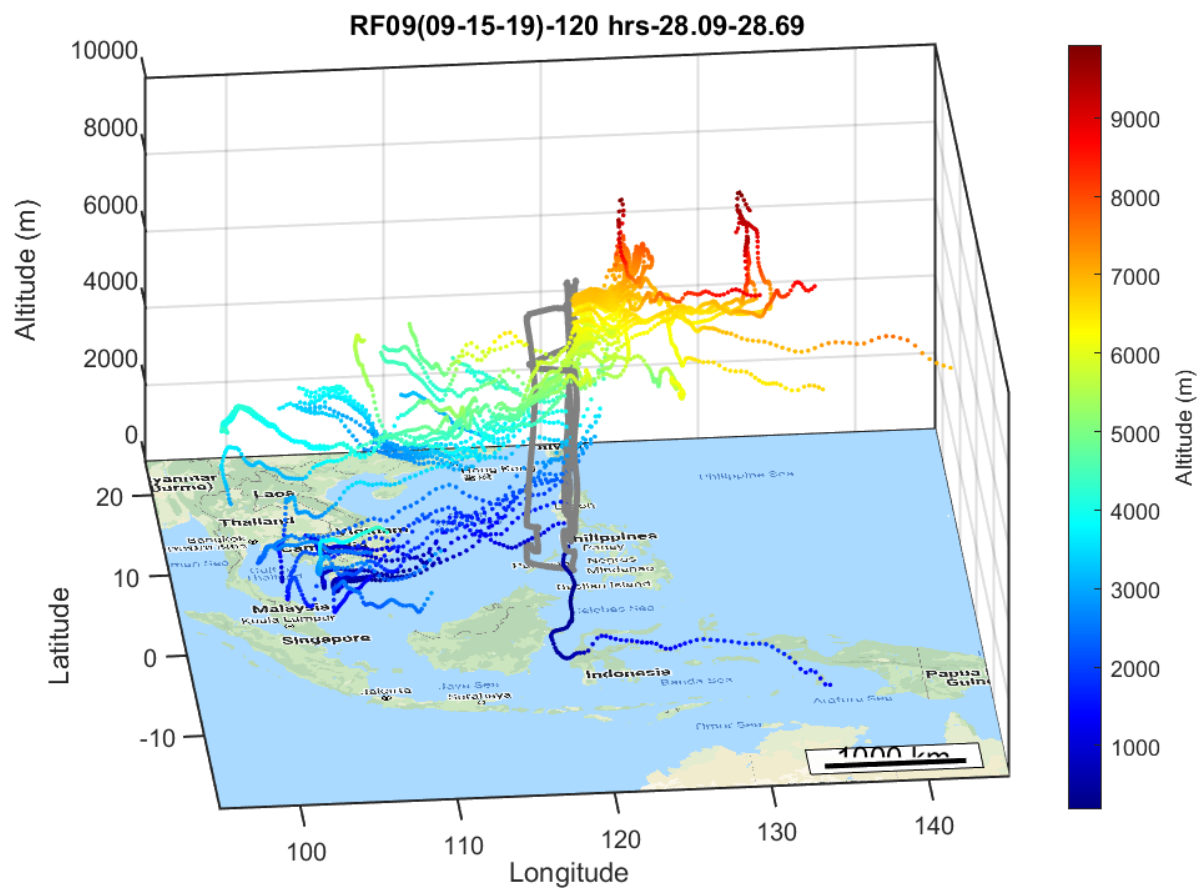
Figure S6. 3-D plot of 120-hour backward trajectories for air masses arriving at the locations where NPF was observed at 6.7 km and along an ascending flight segment, color coded by altitude (meter above sea level). The back-trajectory was initiated every 1 min along the flight track.
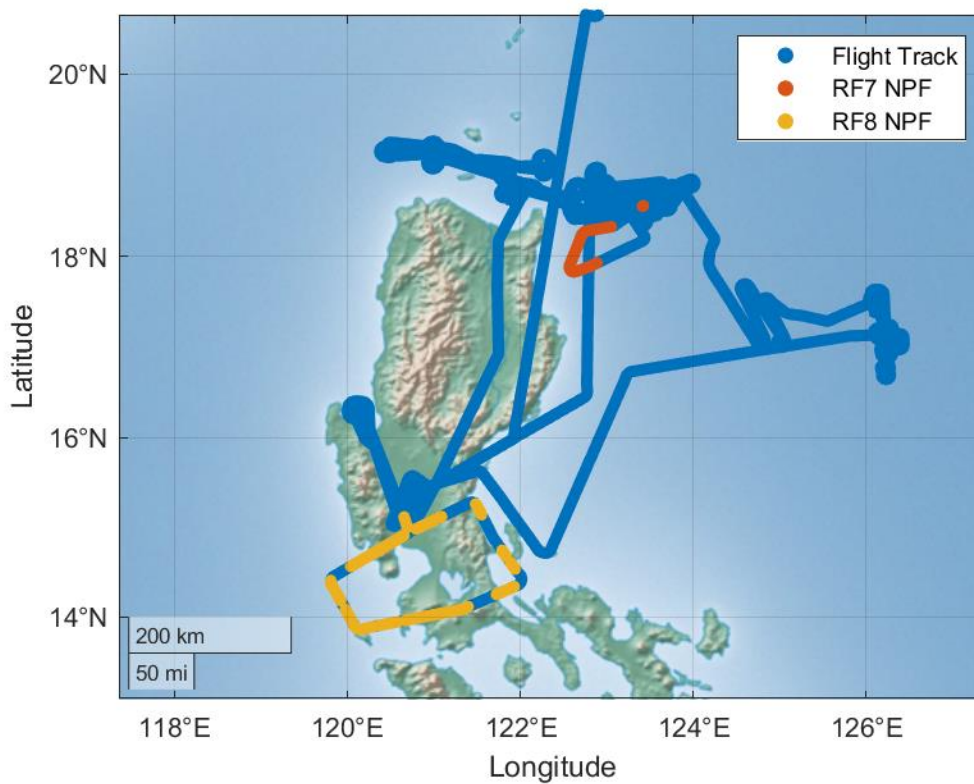
Figure S7. Flight tracks of RF7 (8 September 2019, East of Luzon) and RF8 (13 September 2019, loop around Luzon and Metro Manila). Red and yellow segments represent the urban-influenced NPF events (classified into k-mean cluster #3) during RF7 and RF8, respectively.
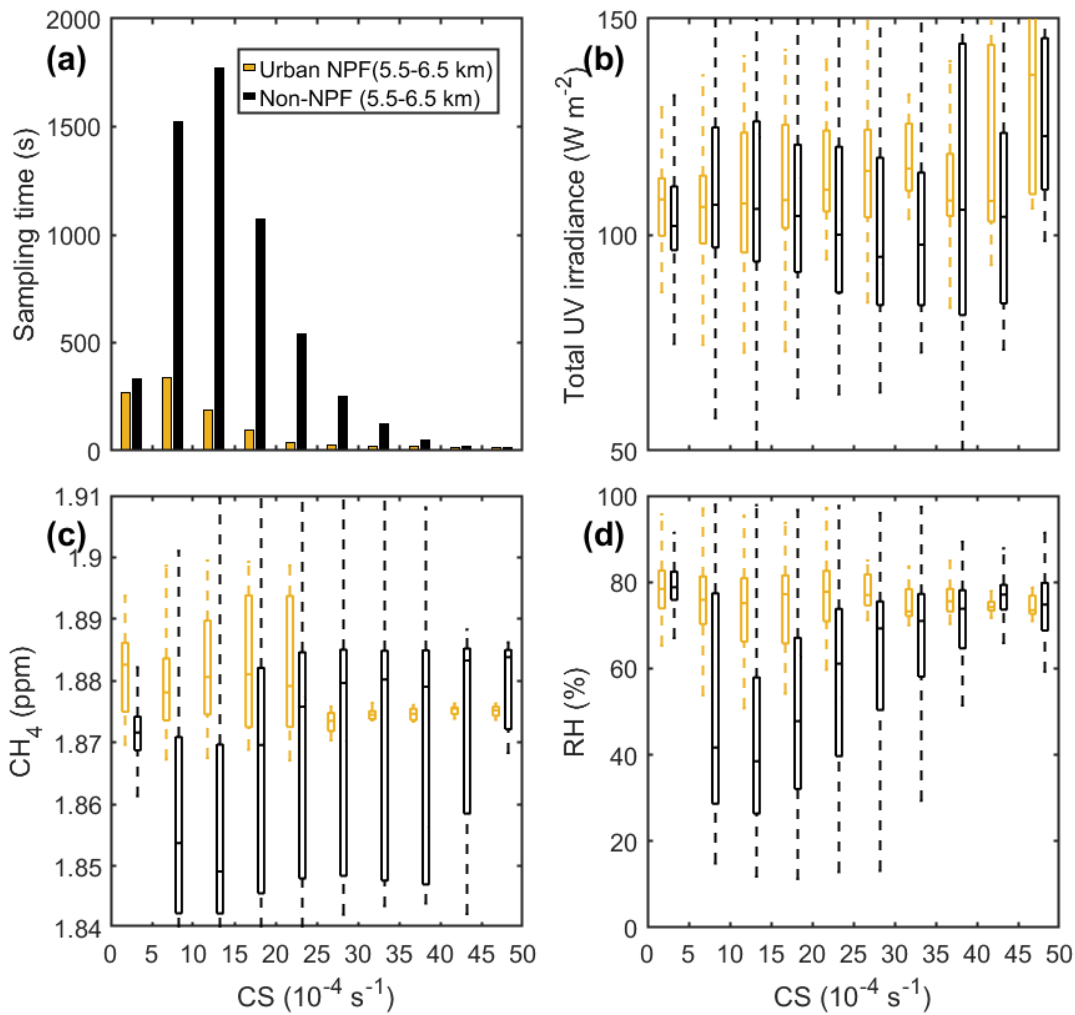
Figure S8. (a) Sampling time, (b) UV irradiance, (c) CH_4, and (d) RH as function of CS for urban-influenced NPF events at 5.5-6.5 km (yellow) and non-NPF periods (black) at the same altitude and time ranges (i.e., to account for altitude dependence of ambient temperature and the dependence of UV irradiance on altitude and time of the day).
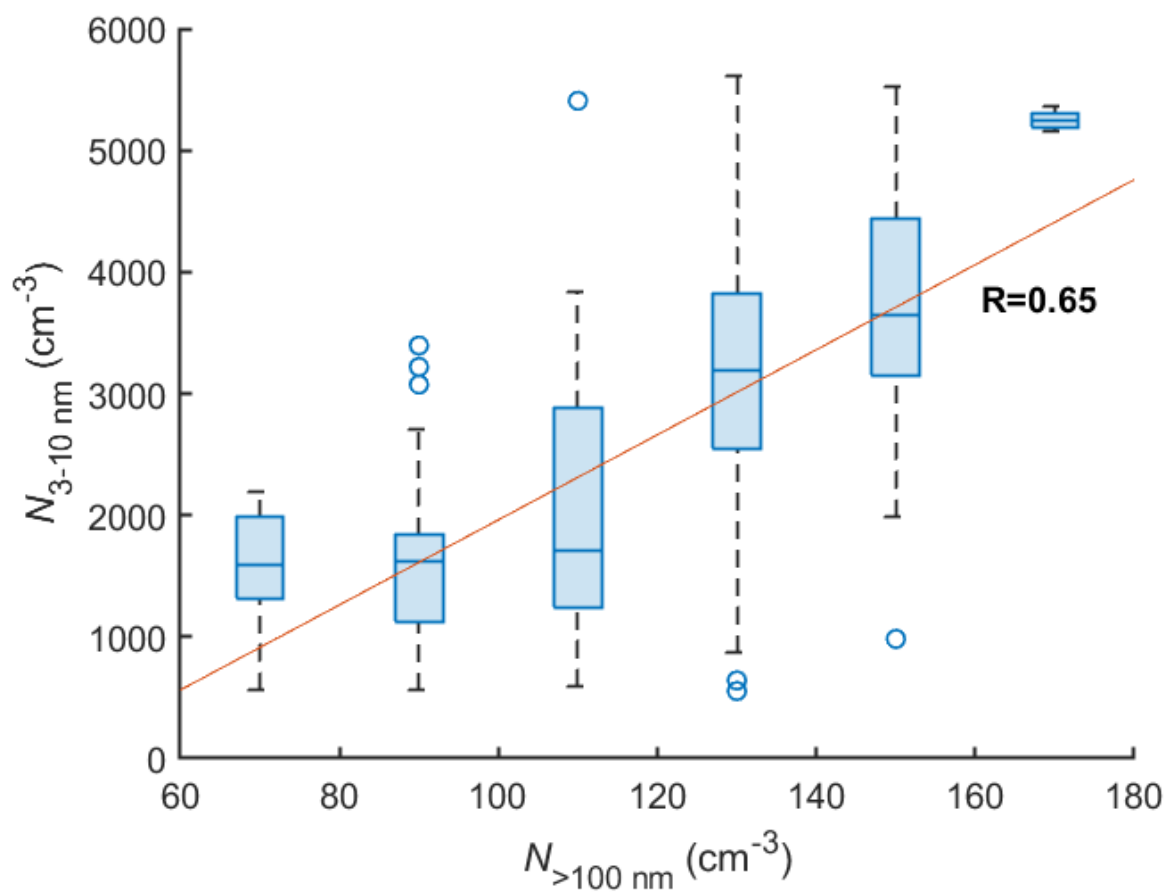
Figure S9. Box whisker plots of $N_{3\text{-}10\,nm}$ for different $N_{>100\,nm}$ bins during the NPF event observed during RF18 (3 October 2019) over Metro Manila. The $N_{>100\,nm}$ bins have a width of 20 cm^{-3} (i.e., 60-80 cm^{-3}, 80-100 cm^{-3} to 160-180 cm^{-3}). Orange line represents a linear fit of all 170 individual data points (R=0.65).

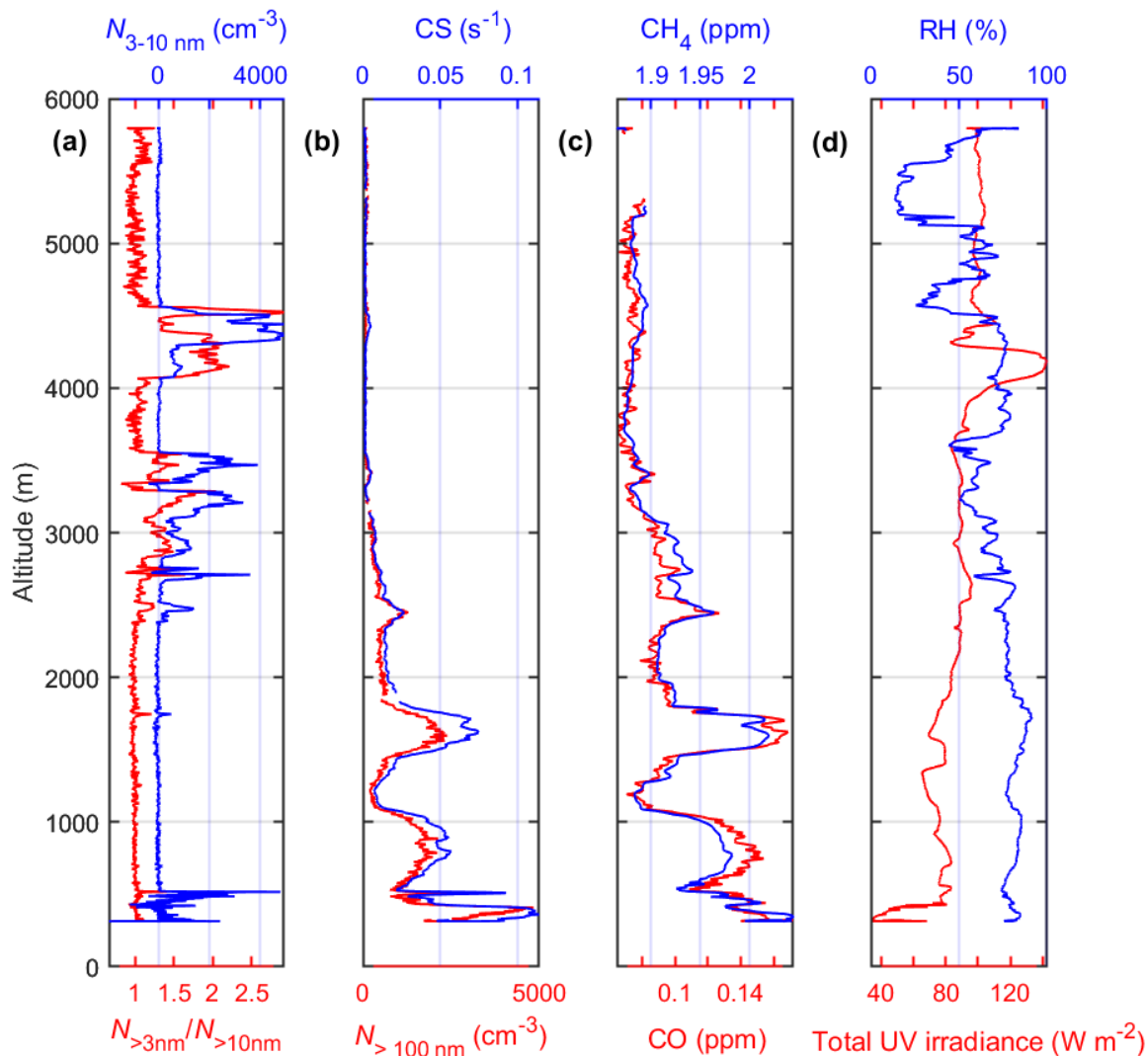Figure S10. Vertical profiles of (a) $N_{>3\,nm}/N_{>10\,nm}$ and $N_{3\text{-}10\,nm}$, (b) CS and $N_{>100\,nm}$, (c) CH_4 and CO, and (d) RH and UV irradiance for a descending flight leg during RF8 (13 September 2019). Only the segment of 4-4.5 km was identified as a NPF event due to its sufficiently long period (i.e., more than 30 seconds). In individual detrainment layers, CS, CO, and CH_4 are locally enhanced, and $N_{3\text{-}10\,nm}$ can be positively correlated with $N_{>100\,nm}$ as observed in the layer around 3.4 km.

Table S1. Overview of P-3B research flights performed during the campaign. The values of altitude, RH, $N_{>3\ nm}/N_{>10\ nm}$, and $N_{3-10\ nm}$ of NPF events identified during each flight are presented as mean value ± standard deviation (σ). Altitude data are reported in meters above sea level.

Date	RF No.	Location	NPF Duration, s	Altitude, m	RH, %	$N_{>3\ nm}/N_{>10\ nm}$	$N_{3-10\ nm}$
08/24/2019	1	Loop around Luzon	108	6090±1598	45.9±19.3	1.43±0.12	493±240
08/27/2019	2	NW Luzon	2140	7119 ±323	71.5±18.7	2.10±0.51	1223±762
08/29/2019	3	Sulu Sea	1340	7642±308	N/A	2.57±1.79	2671±2897
08/30/2019	4	Palawan/ Sulu Sea	5130	7155±1108	80.6±10.2	2.19±1.28	2985±3989
09/04/2019	5	Palawan/ Sulu Sea	360	7630±234	73.3±4.5	2.11±0.73	1435±1311
09/06/2019	6	West Luzon/ Sulu Sea	900	7448±3	86.2±4.7	1.66±2.73	1252±708
09/08/2019	7	East Luzon	2730	6711±758	62.2±19.5	3.86±6.01	842±724
09/13/2019	8	Loop around Luzon	2200	5750±261	78.1±8.8	2.23±1.44	2091±3366
09/15/2019	9	Palawan/ Sulu Sea	880	6741±88	76.1±8.0	4.27±2.05	2607±1901
09/16/2019	10	East Luzon	840	6864±497	68.2±11.1	2.41±1.87	1778±3081
09/19/2019	11	North Luzon	80	6752±2	28.5±1.1	2.25±1.22	1537±1537
09/21/2019	12	North/East Luzon	N/A	N/A	N/A	N/A	N/A
09/23/2019	13	East Luzon	N/A	N/A	N/A	N/A	N/A
09/25/2019	14	East Luzon	N/A	N/A	N/A	N/A	N/A
09/27/2019	15	East Luzon	N/A	N/A	N/A	N/A	N/A
09/29/2019	16	West Luzon	N/A	N/A	N/A	N/A	N/A
10/01/3019	17	West Luzon	N/A	N/A	N/A	N/A	N/A
10/03/2019	18	Manila	170	4827±2	77.8±2.5	2.13±0.47	2288±1409
10/05/2019	19	East Luzon	690	6579±930	59.3±5.8	1.65±0.46	3321±3212

References

Kylling, A., Webb, A. R., Bais, A. F., Blumthaler, M., Schmitt, R., Thiel, S., Kazantzidis, A., Kift, R., Misslbeck, M., Schallhart, B., Schreder, J., Topaloglou, C., Kazadzis, S., and Rimmer, J.: Actinic flux determination from measurements of irradiance, Journal of Geophysical Research: Atmospheres, 108, https://doi.org/10.1029/2002JD003236, 2003.

Nied, J., Jones, M., Seaman, S., Shingler, T., Hair, J., Cairns, B., Gilst, D. V., Bucholtz, A., Schmidt, S., Chellappan, S., Zuidema, P., Van Diedenhoven, B., Sorooshian, A., and Stamnes, S.: A cloud detection neural network for above-aircraft clouds using airborne cameras, Frontiers in Remote Sensing, 4, 10.3389/frsen.2023.1118745, 2023.

Webb, A. R., Bais, A. F., Blumthaler, M., Gobbi, G.-P., Kylling, A., Schmitt, R., Thiel, S., Barnaba, F., Danielsen, T., Junkermann, W., Kazantzidis, A., Kelly, P., Kift, R., Liberti, G. L., Misslbeck, M., Schallhart, B., Schreder, J., and Topaloglou, C.: Measuring Spectral Actinic Flux and Irradiance: Experimental Results from the Actinic Flux Determination from Measurements of Irradiance (ADMIRA) Project, Journal of Atmospheric and Oceanic Technology, 19, 1049-1062, 10.1175/1520-0426(2002)019<1049:Msafai>2.0.Co;2, 2002.